Copyright 2007 Society of Photo-Optical Instrumentation Engineers.
These papers were (will be) published in Proceedings of SPIE, Microlithography and are made available as electronic reprints (preprints) with permission of SPIE. One print or electronic copy may be made for personal use only. Systematic or multiple reproduction, distribution to multiple locations via electronic or other means, duplication of any material in this paper for a fee or for commercial purposes, or modification of the content of the paper are prohibited.

SRAF Placement and Sizing Using Inverse Lithography Technology

Timothy Lin[a*], Frederic Robert[b], Amandine Borjon[b], Gordon Russell[ac], Catherine Martinelli[b], Andrew Moore[a], Yves Rody[b]

[a]Luminescent Technologies, Inc., 2471 E. Bayshore Road, Palo Alto, CA 94303
[b]Crolles2 Alliance, 860 Rue Jean Monnet, 38920 Crolles, France
[c]Current address: Santa Clara, CA 95054

*email: tim@luminescent.com

1.0 Abstract

The use of sub-resolution assist features (SRAFs) is a necessary and effective technique to mitigate the proximity effects resulting from low-k1 imaging with aggressive illumination schemes. This paper investigates the application of one implementation of Inverse Lithography Technology (ILT) to determine optimized SRAF placement and size. In contrast to traditional rule-based methods in which SRAF placement and size are typically predetermined and frozen in place, unmodified during OPC, ILT allows for the simultaneous placement and sizing of SRAFs during target inversion to maximize image quality while also maintaining margin against sidelobe printing. Furthermore, ILT enables SRAF placement for random as well as periodic patterns. In this paper, SRAF placement using this approach is studied through simulations. The computed mask and simulation results are shown to illustrate effectiveness of ILT-generated SRAF features.

Keywords: Optical lithography; Inverse Lithography Technology (ILT); assist features; depth of focus (DOF); Exposure latitude (EL); sub-resolution assist features (SRAF)

2.0 Introduction

The industry has made effective use of aggressive and specialized illumination configurations to improve the printability of low k_1 features. This necessarily entails a tradeoff in the process window of isolated features. Wherever possible, this problem can be mitigated through judicious use of SRAF placement. The implementation of this solution has traditionally been rules based, but there have also been analytical and model based solutions proposed [1-3]. Model based approaches are attractive in that they should naturally adapt to the optical environment obviating the need for complex rules. However, enforcing mask manufacturing constraints, which typically run counter to image quality improvements provided by the use of SRAFs has proven to be difficult. In order to be adopted for widespread usage, a model based approach must be able to find solutions that meet mask making constraints while still providing desired improvements in lithographic quality.

This paper describes the use of ILT to optimize placing and size of SRAFs and its application to a general contact layer design. SRAF placement using ILT is compared to simulation results. For a single contact, the ILT approach is compared with simulation results using a third party simulation package [4]. Then, masks are computed with both conventional and off-axis illumination in order to examine the benefits and compromises

that must be made when utilizing off-axis illumination schemes. The role that SRAFs play in this balancing act is also examined.

3.0 Placement Across Pitch

The following example demonstrates the relationship of SRAF placement to illumination. In this experiment, an isolated contact of is drawn with a ring of 8 SRAFs placed equidistant from the center of the single contact. The drawn size of the main feature is 101 nm. The SRAFs are drawn at 40nm. The distance, d, from the center of the main feature to the center of the SRAF is varied, and the pattern simulated for a given optical condition. Normalized image log slope (NILS) is measured for the main feature at the target CD of 85nm and plotted against SRAF distance; the location of the peak of this curve suggests the optimum placement for an SRAF given a fixed set of optical conditions. Figure 1 shows such a plot for two different illumination types: conventional illumination (σ=0.9) and annular illumination, (σ_{in}/σ_{out}=0.5/0.9). All other imaging conditions were fixed: exposure wavelength (λ) =193 nm, numerical aperture (NA) = 1.2, and mask type was 6% attPSM. This plot shows the degradation of image quality in an isolated contact when employing off-axis illumination. A further observation is that a set of SRAFs placed at key locations can help to recover the image quality of an isolated contact to a level close to that which is obtained when imaging under conventional illumination.

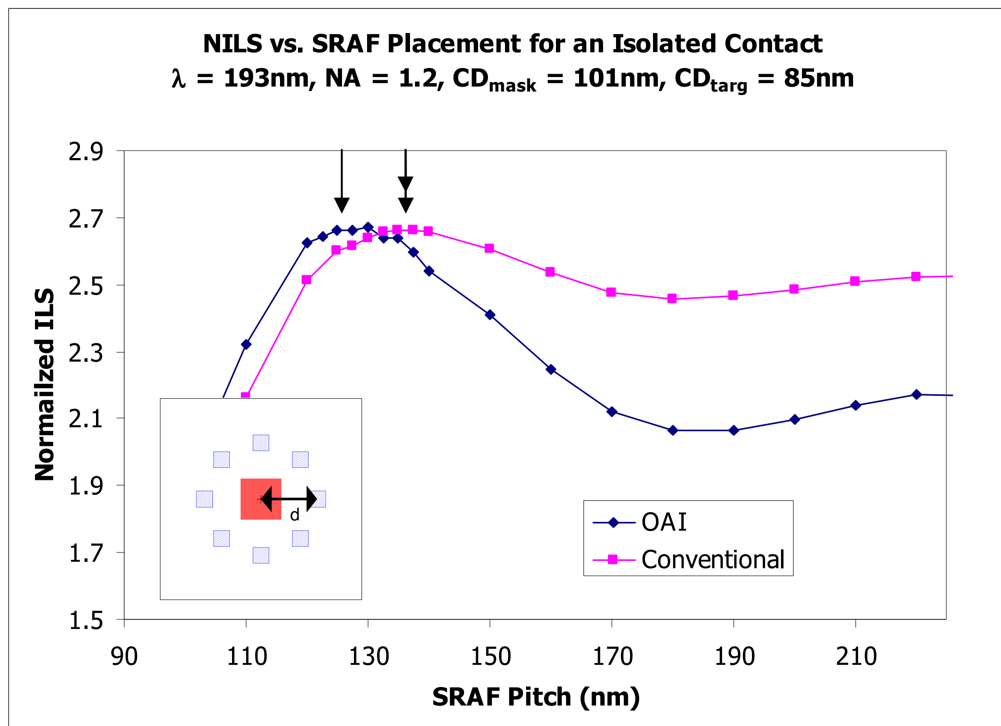

Figure 1. Plot of NILS vs. SRAF Pitch for Off-axis and Conventional Illumination.

As a comparison with the results shown in Figure 1, a mask was computed using ILT for an isolated contact. SRAF placement and size are determined simultaneously with the main feature during inversion. The objective of this exercise was to evaluate how closely the placement of the ILT-computed SRAFs matches the optimum placement for SRAFs

as derived empirically through simulation experiments. In this experiment no manufacturing constraints (width, space, jog, etc.) were employed during the computation of the mask, so as to obtain results unperturbed by the application of these constraints.

Figure 2 shows a comparison of the ILT computed mask using the same annular and conventional illuminations used in the experiment illustrated in Figure 1. Without manufacturing constraints, the SRAF solution is a ring around the main feature. The difference in SRAF placement between the illumination types is also apparent. Mask manufacturing constraints will be addressed in the following section.

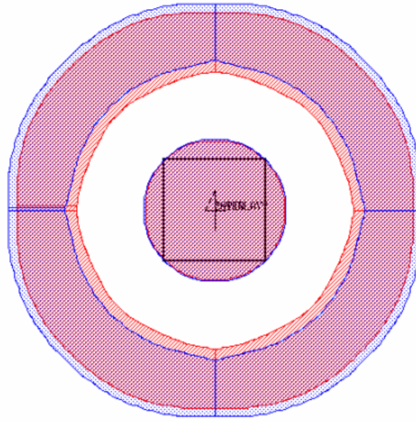

Figure 2. Computed ideal mask for off-axis (red) and conventional (blue) illumination.

Table 1 reports the optimum SRAF placement as determined by ILT (Figure 2) and through forward image simulation (Figure 1). The data indicates qualitative agreement between ILT and the simulation-based approach, with some offset. ILT and simulation-based approaches both place the center of the SRAF closer to the main feature when imaging under off-axis illumination than with conventional illumination. Note that SRAF placement with application to isolated lines was reported in a previous study [5]. In that study there was general agreement between the SRAF placement computed with ILT and SRAF placement as determined empirically through simulation. The data in the previous study also showed an offset between the two approaches. This offset was explained by the fact that in ILT, main feature sizing and SRAF sizing are additional degrees of freedom that can be optimized in tandem with SRAF placement. In the simulation based study illustrated in Figure 1, these factors are fixed.

Illumination/ Placement Method	Off-axis	Conventional
ILT	136	144
Forward Simulation	127[a]	135[b]

Table 1. Comparison of SRAF placement. SRAF placement is measured from center of the main feature to the center of the SRAF. Notes: a) estimated by inspection within a range of 125±5, single in Figure 1. b) estimated by inspection within a range of 135±5, double arrow in Figure 1.

4.0 Mask Manufacturability Constraints

The computation of an ideal mask is an interesting but not practical solution given current mask making capabilities. As such, an SRAF solution must honor requirements for mask manufacturability. Figure 3 shows an example of a mask computed with ILT, but with mask rules enforced. The following manufacturability requirements are enforced during the computation of this mask:

1. Mask segments must be rectilinear.
2. SRAFs must be of minimum width and minimum area.
3. Mask features must meet minimum space and width requirements.
4. Main feature segmentation of the contact should not exceed 3 segments per side.
5. To reduce mask complexity, the SRAFs should be rectangular.
6. To minimize the risk of SRAF printing, SRAFs should not take the shape of "L's" or "T's."

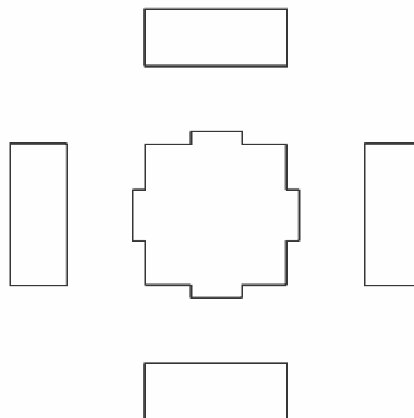

Figure 3. ILT Computed Mask with Mask Rule Constraints.

Besides the Manhattan geometries exhibited, diagonally placed SRAFs are not present in this mask solution. For this example, this represents a conscious tradeoff of sacrificing

some image quality for improved mask manufacturability. The impact of this tradeoff will depend upon the choice of illumination (e.g., annular or quadrupole).

The figures below show an example of mask manufacturing constrains applied during inversion on a real design. Despite the complexity of the design, the inversion computation was successful in maintaining mask rules. It is also interesting to note that this design required the computation to adapt to varying contact pitches and spaces.

Figure 4a shows (circled) the configuration of Figure 3, inside a real design. Assist features for a central contact hole are arranged to the left, right, top and bottom of the drawn contact. Figure 4b illustrates SRAF sharing between contacts, in this case at the lower end of a 1D array. Essentially, the version of ILT under study resolves a conflict between placing two SRAF placements (for the upper and lower contact) by using a single, shared SRAF. In Figure 4c, a much more complex SRAM environment, conflict resolution in SRAF placement is not nearly as intuitive. Considering the circled SRAFs, SRAF 1 assists 4 contacts (3,4,5, and 6), while SRAF 2 assists two (3 and 6).

Variation of SRAF size is allowed in the system under study, as illustrated in the Figure 4d. Contacts 1, 2, and 3 all have four SRAFS (left, right, top and bottom as in Figure 2), but the SRAFs are interleaved. Conflicts are resolved by length modulation. A degree of modulation is required for mask inspectability, but the slight amount of variation makes no practical difference lithographically. Hence variation is evident -- the pairs of circled SRAFs are somewhat different in size (~10 nm), but meet all image quality constraints set up in the inversion. Figure 4e shows a case in which SRAF size variation arises from mask constraints. The upper SRAF (dashed circle) has no neighboring geometries to left or right, and has a horizontal dimension that is about the same as the contact width. The lower SRAF (solid circle) is in conflict with SRAFs to the left and right; the conflict is resolved by means of a shorter horizontal dimension.

Finally, Figures 4f and 4g show two SRAF placements that arise depending on pitch for staggered contacts. In Figure 4f, a long SRAF (circle) effectively acts as a merger of SRAFs for contacts to its upper left and lower right. If Figure 4g, the pitch is higher, and two distinct SRAFs (circle) are placed, one for each of the staggered contacts.

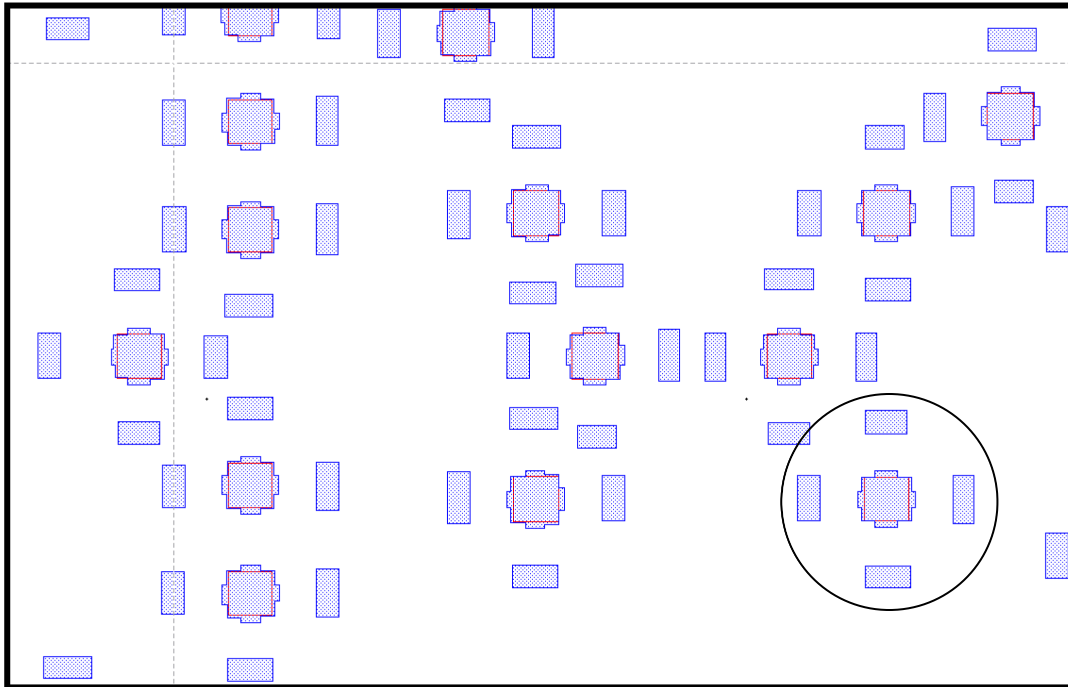

a) Simple case. An isolated contact (circle) has SRAFs at top bottom, left, and right.

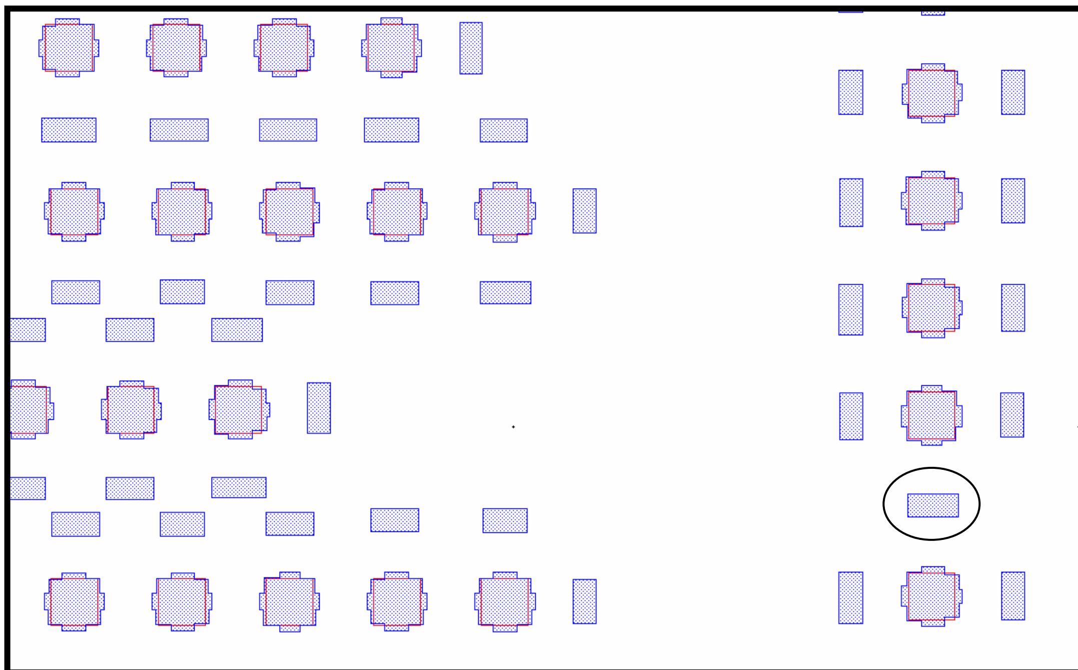

b) One-dimensional arrays. SRAFs run along the side of the array, and between contacts if room is available (circle).

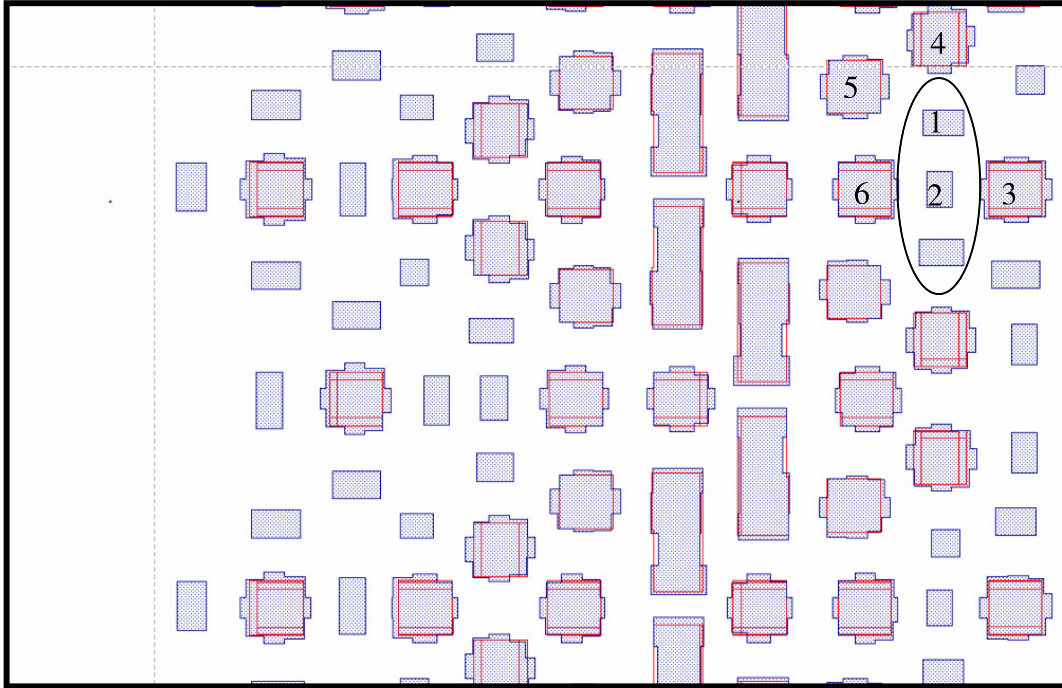

c) Tightly packed case 1, SRAM. The orientation and placement is adaptive according to the surrounding features (circle).

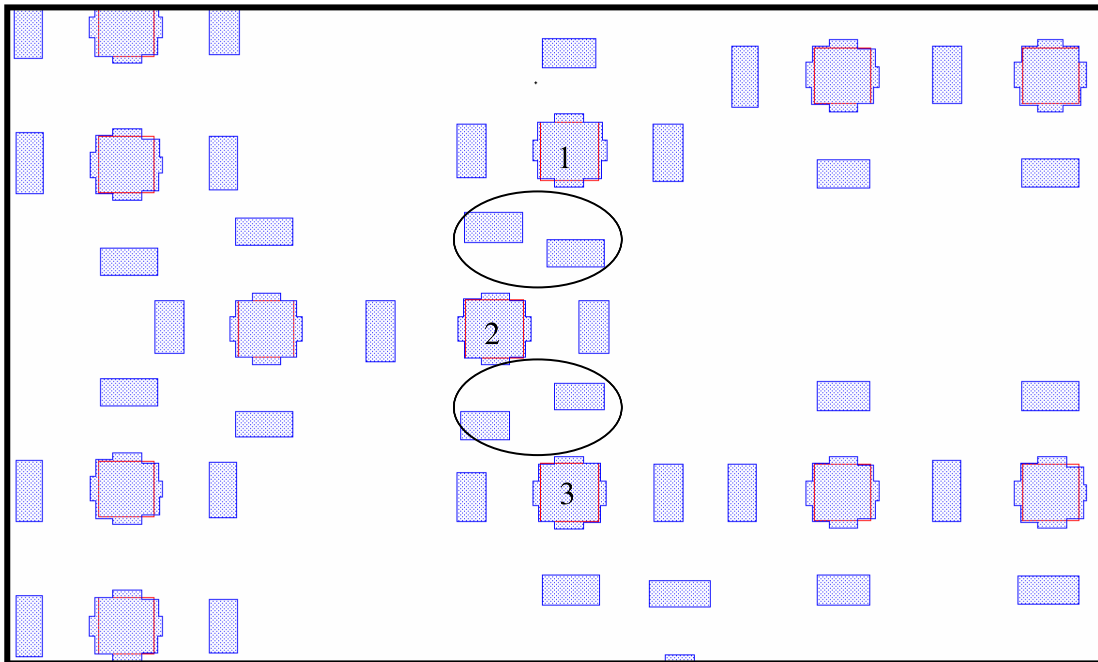

d) Allowed variation. Interdigitation is allowed, and length is modified accordingly. If the exact length does not contribute significantly to image quality, variants may occur (circles).

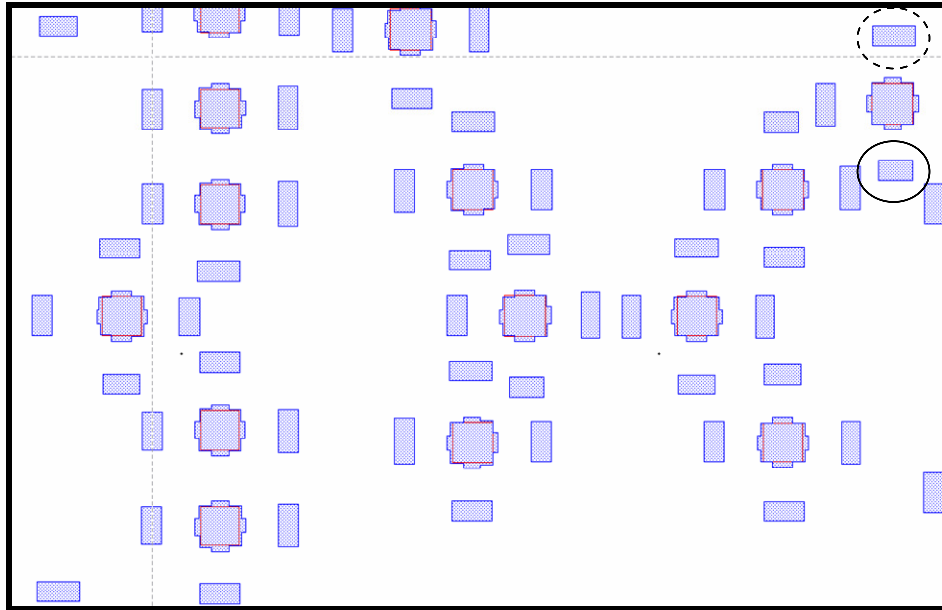

e) Tight packing case 2, logic. Interdigitation may require adaptive shortening of an SRAF in a tight area (circle) such that is smaller than its counterpart (dashed circle).

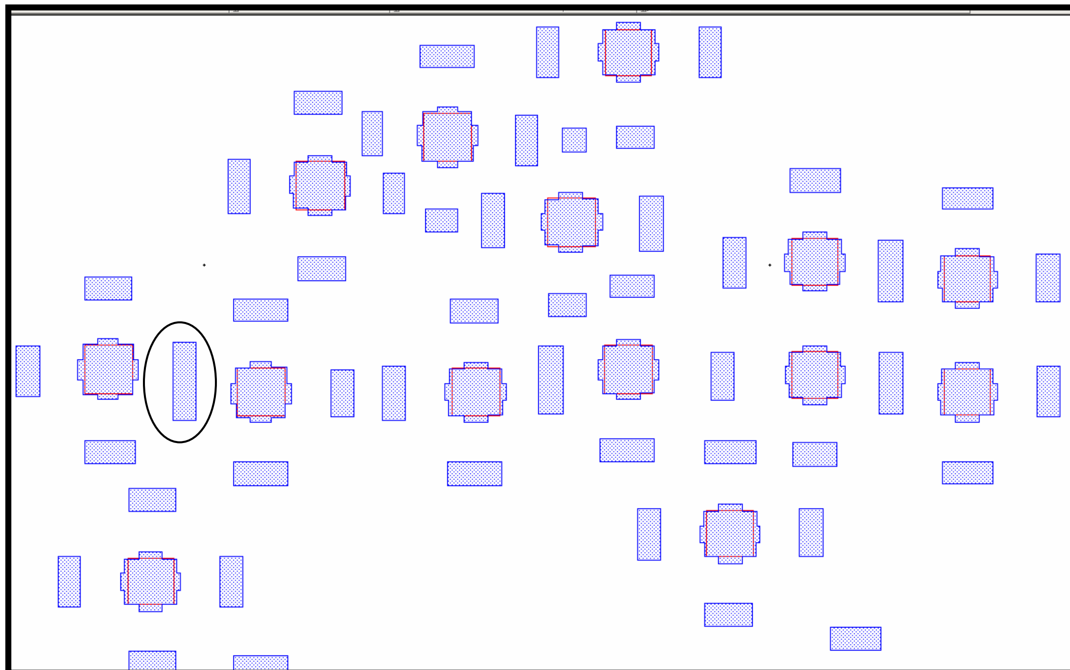

f) Tight packing case 3, logic. SRAFs may be shared between contacts by merging them (circle).

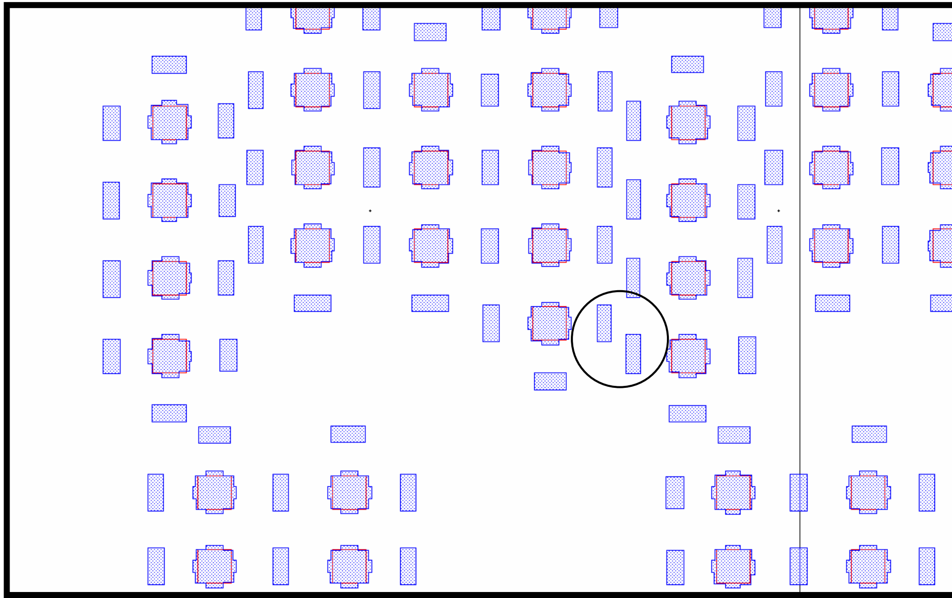

g) Unmerged. In that case of arrays that are shifted relative to each other, and spread apart, merged SRAFs may not be optimal. In this example, the SRAFs are placed in line shifted relative to each other, while meeting mask spacing rules (circle).

Figure 4. Examples from ILT computed masks a) through g).

5.0 Application of ILT SRAFs

The choice of illumination strategy often represents the best compromise available to print all the features in a given design. In a mixed pitch environment, the best illumination scheme for one pitch will likely be sub-optimal for another environment. This is especially true for aggressive off-axis illumination schemes.

To demonstrate the positive and negative impact of off-axis illumination the design shown in Figure 5 was imaged with both off-axis and conventional illumination. The nested contact is the middle contact from a set of 3 contacts placed at minimum pitch in the horizontal direction. This represents a particularly challenging lithographic problem as the spatial frequencies associated with this feature are significantly different in the X and Y direction. Furthermore the pattern has both a nested and isolated component as the edge contacts are isolated on one side. The isolated contact is a single contact at the edge of the design clip placed at a distance greater than $2*(\lambda/NA)$ from its nearest neighbor. In this example, λ=193 nm, NA=1.2, and illumination was varied between annular (σ_{in}/σ_{out}=0.5/0.9) and conventional (σ=0.9). Contrast was measured for both nested and isolated pitches as shown. Figure 6 shows the aerial image intensity across a cut line for nested and isolated pitch contacts and for annular versus conventional illumination. When employing off-axis illumination, the contrast for the nested contact while the contrast for the isolated contact degrades.

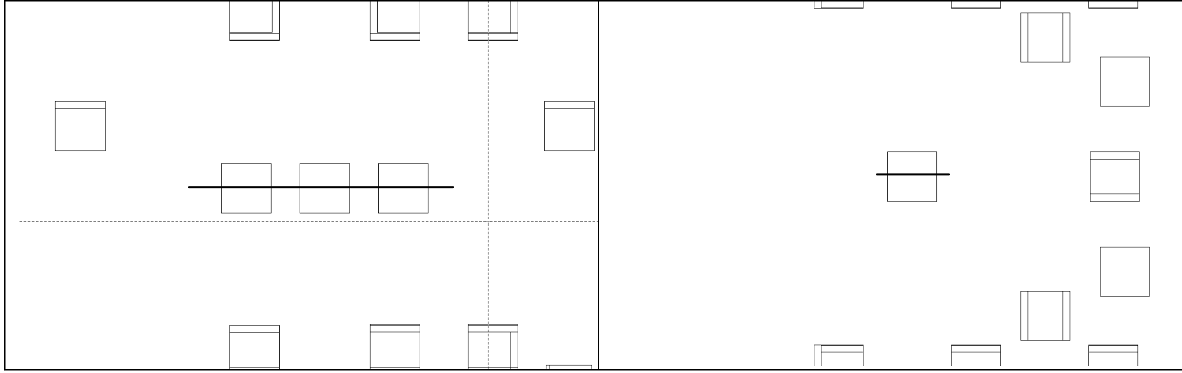

Figure 5. Nested and isolated contact evaluated for contrast.

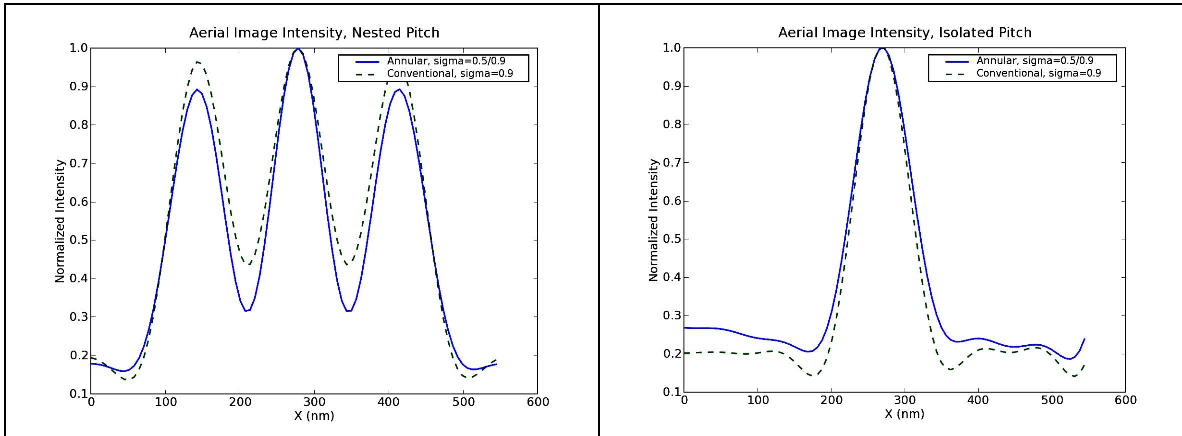

Figure 6. Normalized aerial image intensity for nested and isolated contacts. Annular and conventional illumination are compared.

An ILT mask was then computed for the design and the same locations were measured for image contrast. In the following experiment, a mask employing SRAFs computed with ILT is compared against the same mask in the example above. For this example, the imaging condition for the case of annular illumination from above was used. Figure 7 shows again the aerial image intensities for the nested and isolated contacts, this time comparing annular illumination with and without SRAFs. It is clear to see that the image contrast of the isolated feature was significantly improved with SRAFs.

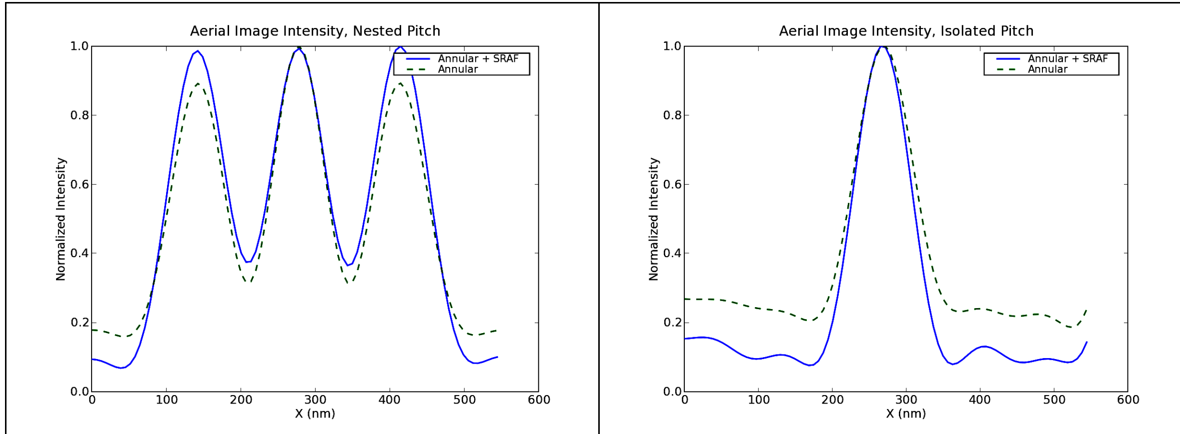

Figure 7. Aerial image intensity for nested and isolated contacts. Annular illumination with SRAF compared without SRAFs. During inversion, images have shifted slightly to meet edge placement requirements.

Next three masks were computed for three imaging conditions: conventional illumination, annular illumination, and annular illumination with SRAFs. Illumination parameters were the same as described above. Instead of contrast, exposure latitude and depth of focus were compared. Results are reported in Table 2. As expected, the best results were obtained for annular illumination with SRAFs. The mask solution computed using annular illumination and SRAFs showed the exposure latitude for both nested and isolated topologies to be comparable to that using conventional illumination. However, in the case of annular illumination, the depth of focus improved by 14%. The use of SRAFs with conventional illumination did not have a significant impact on the results, an observation consistent with graph in Figure 1 (not shown).

Two observations, not immediately apparent in the contrast data, were noted. First, a mask computed and imaged with annular illumination but without SRAFs could not produce a usable process window for the nested contacts. This is attributed to the fact that the nested contacts selected for this comparison, while representing the smallest pitch in the experiment design, are actually isolated in the vertical direction. It is expected that the large difference in spatial frequencies between the horizontal and vertical directions exhibited by such a design presents a significant challenge for a radial symmetric off-axis illumination configuration.

Second, the mask solution computed for conventional illumination resulted in equivalent exposure latitude to that which was computed for annular illumination with SRAFs. This was achieved by the allowing the mask to grow in the vertical direction. It will be shown later that without this degree of freedom, for example in the case of a fully nested design, it is not possible to achieve the same results when using conventional illumination.

Figure 8. ILT mask computed using conventional and annular illumination. Annular illumination employed SRAFs.

PW Metric	Pitch	Conventional	Annular	Annular w/SRAF
Depth of focus(nm)	1D Nested	173.50	0.00	198.50
	Isolated	146.00	127.20	142.50
Exposure Latitude(%)	1D Nested	17.00	4.93	16.70
	Isolated	23.30	19.20	24.60

Table 2. Process window metrics for nested and isolated features. Process window specs are +/- 5nm EPE. Depth of focus is reported at 5% required exposure latitude.

It was noted above that an ILT mask computed using conventional illumination showed equivalent exposure latitude to a mask computed using annular illumination with SRAFs. To investigate this further, a design with a more constrained environment was studied using the same optical conditions as above (Figure 9a). Table 3 reports the simulated process window results after computing a mask for this design under conventional and annular illumination. Note, that the nested region does not allow sufficient space for SRAFs, so image quality in this part of the design is primarily influenced by illumination choice. In this example, a mask computed and imaged using annular illumination improved exposure latitude and depth of focus of the nested feature by 18% and 36% respectively over one using conventional illumination. The results from a semi-isolated contact (nearest neighbor was 1.6 * λ/NA) shown in Figure 9b were slightly improved when using annular illumination.

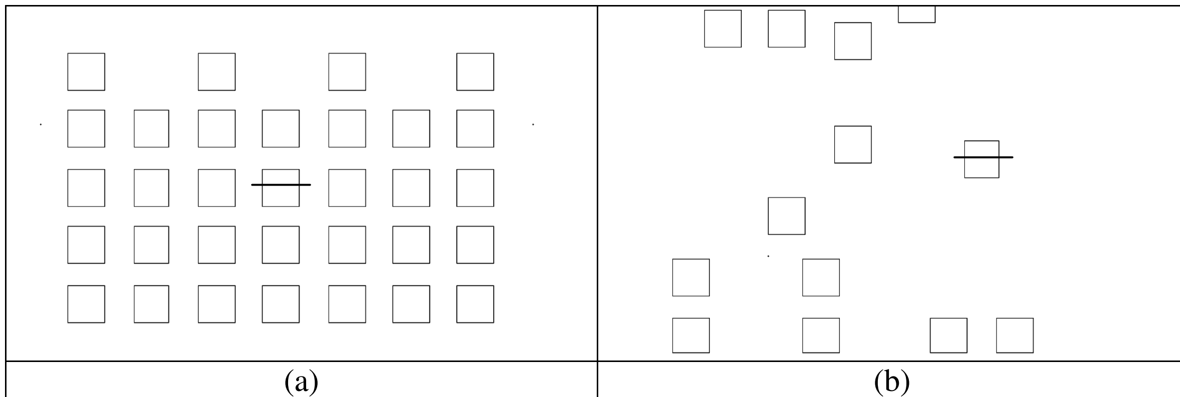

Figure 9. Fully nested (a) and semi-isolated (b) contacts.

PW Metric	Pitch	Conventional	Annular w/SRAF
Depth of Focus(nm)	2D Nested	211.20	286.00
	Isolated	152.70	149.30
Exposure Latitude(%)	2D Nested	12.70	15.00
	Isolated	14.60	21.60

Table 3. Process window metrics for nested and isolated features. Process window specs are +/- 5nm EPE. Depth of focus is reported at 5% required exposure latitude.

The discussion above suggests even another axis of exploration. It can be seen from Table 4 that the improvement in the process window metrics using annular illumination, while significant, could be even larger if more aggressive off-axis schemes such as quadrupole were selected. It is important to note, however, that the use of such an off-axis scheme would require additional design restrictions governing the layout of the nested contacts. This preliminary discussion serves only to suggest that additional optimization choices are available in the development of a patterning solution.

PW Metric	Pitch	Quad
DOF	2D Nested	326.00
	Isolated	198.00
EL	Nested	24.80
	Isolated	20.80

Table 4. Process window metrics for a quadrupole illumination. Process window specs are for +/- 5nm EPE. Depth of focus reported at 5% exposure latitude.

6.0 Conclusion

In this study, the efficacy of an ILT-based approach to SRAF placement was examined. SRAF placement using ILT was shown to be in close agreement with a simulation-based approach, with minor differences attributable to simultaneous optimization of size and placement in the ILT based approach. Constraints for mask manufacturability requirements were addressed where an ideal SRAF solution was constrained to have only Manhattan features. Examples from a complex layout show that mask manufacturability requirements can be applied across a diverse set of topologies, where through-pitch adaptability and conflict resolution are required. The concepts above were then applied to a 45nm contact design to determine if an annular illumination solution could improve the image quality of the nested contacts while using SRAFs to maintain or even improve the printability of the isolated contacts. These simulation experiments showed that this objective was achieved.

References

1. S. Manakli, Y. Trouiller, P. Schiavone, Y. Rody, P.-J. Goirand, "Optimization of the depth of focus based on the analysis of the diffraction orders in the pupil plane," **Microelectronic Engineering vol. 67-68**., pp. 70-77 (2003)

2. Robert Socha, Douglas Van Den Broeke, Stephen Hsu, J. Fung Chen, Tom Laidig, Noel Corcoran, Uwe Hollerbach, Kurt E. Wampler, Xuelong Shi, Will Conley, "Contact hole reticle optimization using interference mapping lithography (IMLtm)," **Proc. SPIE vol. 5446**, pp.516-524 (2004)

3. Shumay D. Shang, Yuri Granik, Lisa Swallow, Li-guo Zhang, Travis Brist, Andres Torres, Chi-Yuan Hung, Qingwei Liu, "Model-based insertion and optimization of assist features with application to contact layers," **Proc. SPIE vol. 5992**, pp.1Y1-1Y10 (2005)

4. Simulations performed using Panoramic EM-Suite.

5. Andrew Moore, Timothy Lin , Yong Liu, Gordon Russell, Linyong Pang, Daniel Abrams, “Inverse Lithography Technology at Low k1: Placement and Accuracy of Assist Features,” **Bacus Symposium on Photomask Technology vol. 6349**, pp. 4T1-4T11 (2006)

6. Daniel Abrams, Linyong Pang, “Fast Inverse Lithography Technology,” **Proc. SPIE vol. 6154**, pp. 1J1-1J9 (2006)